ISSN 0021-3640, JETP Letters, 2023, Vol. 117, No. 10, pp. 742–746. © The Author(s), 2023. This article is an open access publication.
Russian Text © The Author(s), 2023, published in Pis'ma v Zhurnal Eksperimental'noi i Teoreticheskoi Fiziki, 2023, Vol. 117, No. 10, pp. 740–745.

OPTICS
AND LASER PHYSICS

Quasicrystalline Structures with Narrow-Band Frequency–Angular Selectivity

V. A. Chistyakov[a, *], M. S. Sidorenko[a], A. D. Sayanskiy[a], and M. V. Rybin[a, b]

[a] *Faculty of Physics, ITMO University, St. Petersburg, 191101 Russia*

[b] *Ioffe Institute, St. Petersburg, 194021 Russia*

**e-mail: v.chistyakov@metalab.ifmo.ru*

Received March 22, 2023; revised April 12, 2023; accepted April 17, 2023

Design methods in the reciprocal space allow one to obtain structures with desired properties. Quasicrystalline photonic structures, which ensure the selective scattering of an electromagnetic wave incident on the sample, have been designed. The maxima of the Fourier transform of the desired distribution of the permittivity in the reciprocal space are located along two arcs on the Ewald sphere, which corresponds to the scattering of the wave with the required wavelength and angle of incidence. The material distribution has been determined by the transition to the real space. A structure with a low dielectric contrast has been formed after the binarization of the refractive index. The theoretical analysis of the properties of the structure has confirmed the frequency–angular selectivity of scattering. The numerical calculations show the possibility of achieving the effective scattering and absorption of the electromagnetic energy up to 94% in a narrow frequency range and in a narrow interval of angles of incidence at a dielectric contrast of two materials of 1.07.

DOI: 10.1134/S0021364023601215

Photonic crystals [1–3] and other resonance structures [4–6], which ensure the possibility of controlling electromagnetic radiation, have become widespread in the last decades. The key property of photonic crystals is the existence of a band gap caused by the Bragg scattering from crystal layers in structures with periodically varying refractive indices. However, the periodicity of a photonic crystal restricts the number of possible symmetries forming a fixed number of possible space groups.

Intuitive methods for the development of photonic structures are changed to the inverse design methods with the use of numerical optimization, including artificial intelligence [7–11]. These methods lead to a complex spatial distribution of a material, but these structures have the required functionality. The achievements of additive digital technologies allowed the fabrication of numerous photonic structures with a more complex structure than photonic crystals such as hyperuniform structures [12, 13], quasicrystals [14], moiré gratings [15], and Fourier surfaces [16].

A quasicrystalline structure that has a full band gap at a low dielectric contrast, which can be reached using polymeric materials, has recently been demonstrated in [17] using the reciprocal space design. Such structures in the real space correspond to the superposition of numerous gratings with the uniform distribution of orientations in the total solid angle 4π. It was demonstrated that the absence of the translational symmetry in ordered two-dimensional quasicrystalline structures does not affect the modulation of the local density of states of the electromagnetic field [18]. In addition, studies of the localization of waves in aperiodic systems are of interest [19–23]. One of the most intriguing properties of disordered structures is the Anderson localization [24], which is observed in numerous structures [25, 26]. The internal light localization in a three-dimensional icosahedral quasicrystal has been observed in the recent experiment [14]. Effects of scattering and localization in aperiodic structures occur in a broad frequency band and for various directions. At the same time, the possibility of the fabrication of a structure selectively scattering the wave in a given direction and at given frequencies has not yet been reported [27].

In this work, using the inverse design method, we fabricate low-contrast quasicrystalline structures with the frequency–angular selectivity of the scattering of the incident electromagnetic field. Using the Ewald sphere, we specify a certain function in the reciprocal space whose nonzero values or *maxima* are located so that the radiation at a certain wavelength in a certain direction is efficiently scattered from the sample. The calculations of the propagation of the electromagnetic wave in the sample with a realistic absorption coefficient of the material completely confirm the expected effect.

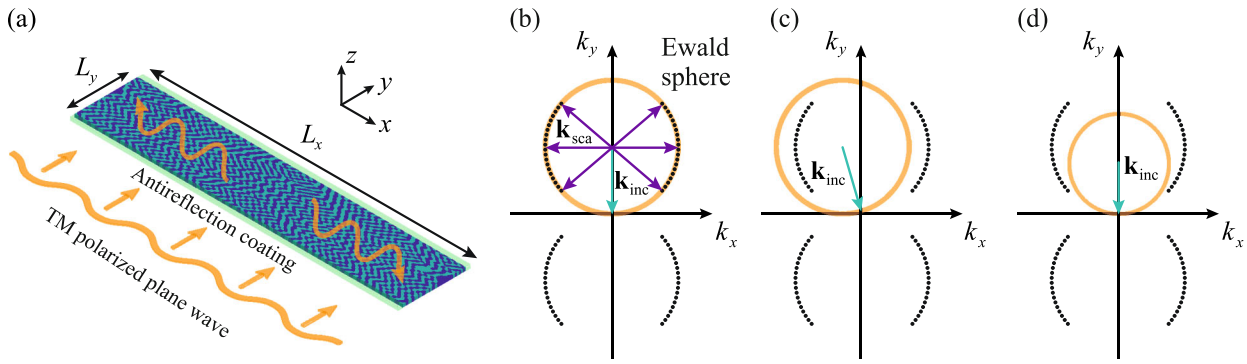

Fig. 1. (Color online) (a) Sketch of the quasicrystalline structure in the real space generated using 40 maxima in the reciprocal space. The lengths of the sides in the longitudinal and transverse sections are $L_y = 10\lambda_0$ and $L_x = 50\lambda_0$, where λ_0 is the working wavelength. (b) (Orange line) Ewald sphere at the normal incidence of the wave with the wave vector $\mathbf{k}_{inc}$ passes through (black points) the maxima in the reciprocal space, which results in the effective scattering of the wave $\mathbf{k}_{sca}$ in the transverse direction. (c) Ewald sphere at the oblique incidence of the wave with the wave vector $\mathbf{k}_{inc}$ corresponding to the absence of scattering. (d) Ewald sphere at the normal incidence of the wave and at a long wavelength corresponding to the absence of scattering.

Scattering in electromagnetic problems is specified by the spatial distribution of the permittivity $\varepsilon(\mathbf{r})$. To determine the quasicrystalline structures with desired properties, we used the reciprocal space design [28]. We recall that the scattering of the incident wave with the wave vector $\mathbf{k}_{inc}$ to the wave with the wave vector $\mathbf{k}_{sca}$ in low-contrast dielectric structures depends on the intensity of the Fourier transform $\varepsilon(\mathbf{r})$ at the point with the position vector $\mathbf{k}_{sca} - \mathbf{k}_{inc}$ in the reciprocal space. To determine the conditions for scattering, it is convenient to use the Ewald sphere with the radius $k_0 = |\mathbf{k}_{inc}|$ and the center at $-\mathbf{k}_{inc}$, which specifies all possible directions of elastic scattering. If the maximum of the Fourier transform of $\varepsilon(\mathbf{r})$ is on the Ewald sphere, scattering occurs in the corresponding direction. The Ewald sphere for the problem under consideration is a circle. We specify maxima along arcs of the circle in the reciprocal space, which determine the scattering of the normally incident wave. Thus, scattered waves will propagate in the sample in sectors formed by these arcs (Fig. 1b). Figures 1c and 1d qualitatively present the cases of the deviation of the angle of incidence from the normal and the deviation from a given wavelength. It is seen that the Ewald sphere in these cases does not pass through maxima and effective scattering does not occur, and the structure is transparent.

The distribution of the refractive index in the real space was obtained by the Fourier transform. For the distribution in the real space to be real-valued, maxima in the reciprocal space should be located symmetrically with respect to the origin of coordinates. This additional condition is responsible for additional maxima in the lower half-plane (Figs. 1b–1d).

It is technically more convenient to specify the permittivity distribution in the real space by means of a set of superimposed sinusoidal functions [17, 18]. To this end, a set of maxima corresponding to the parameters of these gratings is formed on arcs of the circle with the radius specified by the required wavelength λ_0. We suggest that maxima are located only in the arcs $[-\alpha_c, \alpha_c]$, where $\alpha_c = 1/\bar{n}$ and $\bar{n}$ is the average refractive index of the medium. Images of the gratings whose directions and periods are specified according to maxima distributed along the arcs are shown in Fig. 2a. In this case, the distribution of the material of the quasicrystalline structure is specified by the superposition of one-dimensional sinusoidal gratings (Fig. 2b):

$$\Delta n_g(\mathbf{r}) = \sum_{i=1}^{N} \Delta n_i \cos(\mathbf{g_i} \cdot \mathbf{r} + \varphi_i), \quad (1)$$

where Δn_i is the modulation amplitude of the refractive index for the ith grating, N is the total number of gratings on the circle in the upper half-plane, $\mathbf{g}_i$ is the normal unit vector to the ith grating, and φ_i is the random phase. It is noteworthy that a singularity, which can lead to undesired effects, appears at the origin of coordinates when the phases of all gratings are the same. Random phases shift this singularity far beyond the sample.

To obtain the structure consisting only of two dielectric materials, we applied the binarization of the continuous refractive index $\Delta n_g(\mathbf{r})$:

$$n_b(\mathbf{r}) = \bar{n} + \Delta n \operatorname{sgn}[\Delta n_g(\mathbf{r})], \quad (2)$$

where Δn is the deviation of the refractive index from the average value $\bar{n}$. As a result, the quasicrystalline structure with desired properties can be fabricated from two materials with the refractive indices $n_1 = \bar{n} + \Delta n$ and $n_2 = \bar{n} - \Delta n$. An example of such a structure is presented in Fig. 2c.

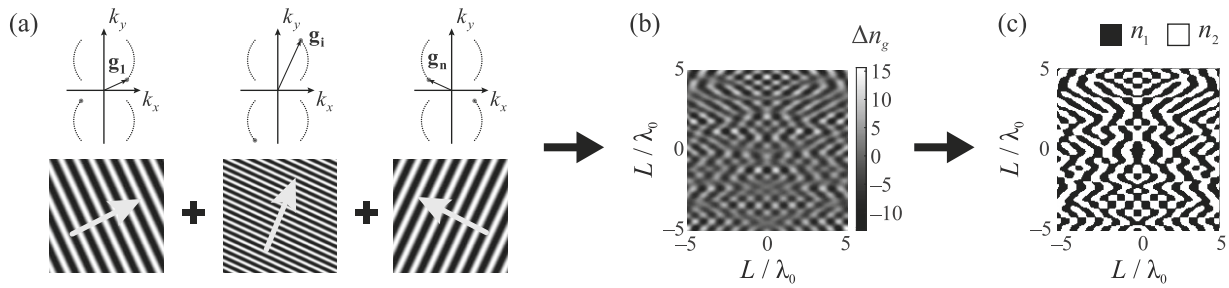

Fig. 2. (a) Illustration of the calculation of the distribution of the refractive index by the superposition of sinusoidal functions corresponding to the maxima of the Fourier transform of $\varepsilon(\mathbf{r})$ in the reciprocal space. (b) Image of the structure with a continuous distribution of the refractive index generated using 40 maxima. (c) Image of the structure after the binarization of the refractive index.

The Bloch theorem cannot be used to study aperiodic structures; therefore, it is necessary to examine full-sized structures. In this work, we study the two-dimensional quasicrystalline structure, which can be implemented experimentally for TM-polarized electromagnetic radiation, by placing the sample in the plane-parallel metallic waveguide. Figure 1a schematically shows the quasicrystalline structure generated using Eqs. (1) and (2) for 40 gratings. The structure has the sizes $L_x = 50\lambda_0$ and $L_y = 10\lambda_0$, where $\lambda_0 = 2\pi/k_0$ is the working wavelength at which the normally incident electromagnetic wave should be efficiently scattered. The structure consists of the materials with the refractive indices $n_1 = 1.48$ and $n_2 = 1.58$, which correspond to easily available polymeric materials used for three-dimensional printing [29, 30]. The technological process allows one to locally vary the density of the printed material, which ensures the dielectric contrast. We also take into account absorption in both materials $\tan\delta = 0.003$. It is important that the described results only quantitatively depend on the choice of the refractive indices and the contrast. Periodic boundary conditions used along the x axis make it possible to obtain results for extended structures. A quarter-wave antireflection coating was deposited at the boundaries through which incident radiation passed in order to minimize undesired scattering at the transmission through the interface between two media. The environment for structures is air with a refractive index close to 1; hence, the refractive index for the antireflection coating is $n_c = \sqrt{\bar{n}}$ and the thickness of the layer is $L_c = \lambda_0/4n_c$.

The calculations were performed using the CST Studio Suite for the simulation of the propagation of electromagnetic waves. Figure 3a presents the transmittance, T, and reflectance, R, spectra at normal incidence. The transmittance spectrum demonstrates a sharp dip in a band near the dimensionless frequency $\lambda_0/\lambda = 1$ against the background of an almost perfect transmittance beyond the band. The reflectance in the entire range is no more than 0.1. The wave scattered in the transverse direction propagates in the sample until it is absorbed or rescattered in the transmission or reflection direction. To determine the quantitative characteristics of the quasicrystalline structure, we consider the *captured* energy. According to the energy conservation law, the absorbed energy is $A = 1 - T - R$. The absorption spectrum has a peak at wavelengths $\lambda \approx \lambda_0$ corresponding to the stop band of the structure (Fig. 3b). The maximum absorption in the peak is 94%. Thus, the quasicrystalline structure demonstrates a pronounced spectral selectivity of absorption.

We now examine the angular selectivity of the proposed quasicrystalline structure. Periodic boundary conditions used to extend the sample make it possible to specify the incident wave propagating along the y axis. The period of the computational region for the case of oblique incidence depends on the wavelength. For this reason, we rotate the structure itself in the reciprocal space by the angle θ, leaving the outer boundary unchanged, instead of the variation of the angle of incidence. The results obtained in this approach are not qualitatively different from those obtained with the variation of the angle of incidence of the wave on the sample.

Figure 4a shows the $(\theta, \lambda_0/\lambda)$ map of the transmittance, where θ is the angle of the axes in the reciprocal

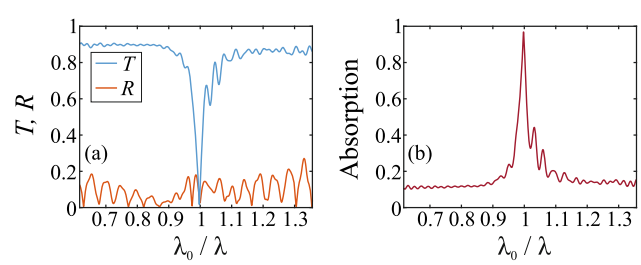

Fig. 3. (Color online) (a) (Blue line) Transmission and (orange line) reflection coefficients versus the dimensionless frequency λ_0/λ at the normal incidence of the TM wave. (b) Absorption coefficient versus the dimensionless frequency λ_0/λ at the normal incidence of the TM wave.

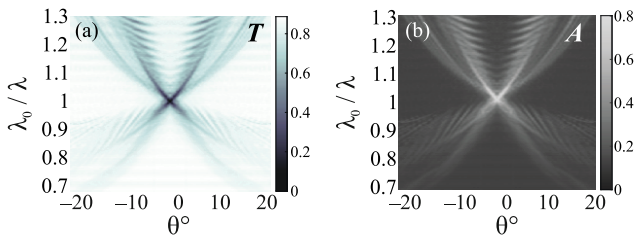

Fig. 4. (Color online) (θ, λ_0/λ) maps of the (a) transmittance and (b) absorbance, where θ is the angle of the axes in the reciprocal space with respect to the edges of the sample and λ_0/λ is the dimensionless frequency.

space with respect to the edges of the sample and λ_0/λ is the dimensionless frequency. It is seen that the minimum transmittance corresponds to the wavelength $\lambda = \lambda_0$ and $\theta = 0°$. Under the variation of the angle of observation, the dip is split into two bands, which are rapidly weakened and almost vanish at angles $\theta > 10°$. Figure 4b shows the (θ, λ_0/λ) map of the absorbance. It is seen that the features in the transmission and absorption spectra coincide with each other.

The behavior of spectral features is in good agreement with the model based on the Ewald sphere. The normally incident wave is scattered only under the condition $\lambda = \lambda_0$ when the Ewald sphere passes through all maxima along two arcs (see Fig. 1). The variation of the wavelength corresponds to the variation of the Ewald sphere and violates the condition of passage through the maxima. Maxima in the reciprocal space for finite samples are smoothed because of the coordinate–momentum uncertainty relation. At a small deviation from normal incidence, only some maxima in the reciprocal space remain on the Ewald sphere. As a result, transmittance spectra for nonzero angles of incidence include two dips, which correspond to one of the maxima lying on the large Ewald sphere and another maximum falling on the small Ewald sphere. Since some maxima are beyond the Ewald sphere, the efficiency of the total scattering of the incident wave decreases, leading to the degradation of spectral features observed in Fig. 4a.

To confirm the selective scattering of the electromagnetic wave in the transverse direction, we calculated the Poynting vector. Figure 5 presents the distribution of the magnitude and direction of the Poynting vector in the sample for three wavelengths. The structure is transparent to wavelengths $\lambda_0 = 0.9\lambda$ (Fig. 5a) and $\lambda_0 = 1.1\lambda$ (Fig. 5c), and the direction of the Poynting vector corresponds on average to the direction of incidence. The picture for the working wavelength $\lambda = \lambda_0$ is different (Fig. 5b). The sample redirects the energy of the incident wave in the perpendicular direction, as suggested in the design of the quasicrystalline structure in the reciprocal space using the Ewald sphere.

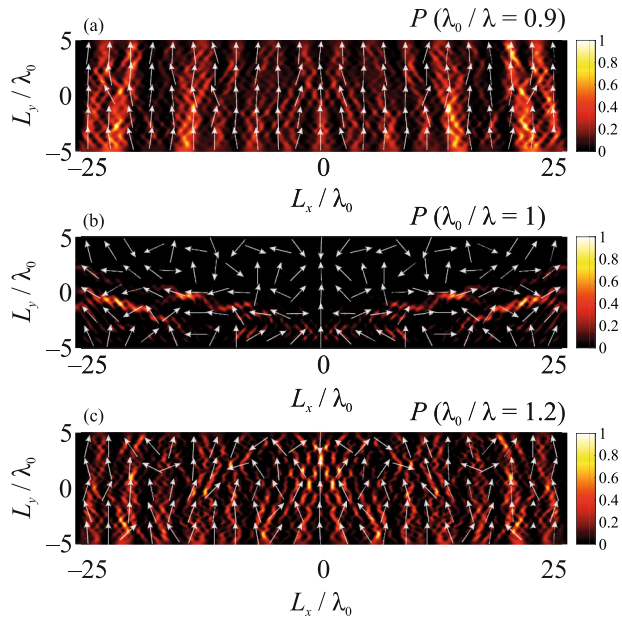

Fig. 5. (Color online) Normalized power flux intensity of the electromagnetic field in the structure in the case of the normal incidence of the TM-polarized plane wave at λ_0/λ = (a) 0.9, (b) 1, and (c) 1.1. White arrows indicate the direction of the flow.

To summarize, we have presented the quasicrystalline structure with the frequency–angular selectivity of scattering of electromagnetic waves designed in the reciprocal space. The uniform distribution of maxima in circle arcs in the reciprocal space corresponds to a set of gratings in the real space. Scattering and subsequent absorption of electromagnetic waves in such a structure are observed only at a given angle of incidence and at a certain frequency. We have shown that a selective absorption up to 94% can be achieved at a low contrast of materials of 1.07. The distribution of the electromagnetic power flow in the plane of the structure has demonstrated a directional energy transfer along the structures only at a given wavelength. We expect that the proposed quasicrystalline structures will provide broad possibilities for the fabrication of new photonic devices with unique properties.

ACKNOWLEDGMENTS

We are grateful to A.Yu. Petrov for the discussion of the idea of this work.

FUNDING

This work was supported by the Russian Science Foundation, project no. 20-79-10316.

CONFLICT OF INTEREST

The authors declare that they have no conflicts of interest.

REFERENCES

1. E. Yablonovitch, Phys. Rev. Lett. **58**, 2059 (1987).
2. J. D. Joannopoulos, P. R. Villeneuve, and S. Fan, Nature (London, U.K.) **386**, 143 (1997).
3. J. D. Joannopoulos, S. G. Johnson, J. N. Winn, and R. D. Meade, *Photonic Crystals: Molding the Flow of Light* (Princeton Univ. Press, Princeton, NJ, 2008).
4. M. V. Rybin and M. F. Limonov, Phys. Usp. **62**, 823 (2019).
5. P. Tonkaev and Y. Kivshar, JETP Lett. **112**, 615 (2020).
6. A. M. Chernyak, M. G. Barsukova, A. S. Shorokhov, A. I. Musorin, and A. A. Fedyanin, JETP Lett. **111**, 46 (2020).
7. S. Molesky, Z. Lin, A. Y. Piggott, W. Jin, J. Vuckovic, and A. W. Rodriguez, Nat. Photon. **12**, 659 (2018).
8. M. M. R. Elsawy, S. Lanteri, R. Duvigneau, J. A. Fan, and P. Genevet, Laser Photon. Rev. **14**, 1900445 (2020).
9. K. R. Safronov, V. O. Bessonov, and A. A. Fedyanin, JETP Lett. **114**, 321 (2021).
10. P. R. Wiecha, A. Arbouet, C. Girard, and O. L. Muskens, Photon. Nanostruct.: Fundam. Appl. **9**, B182 (2021).
11. P. R. Wiecha, A. Y. Petrov, P. Genevet, and A. Bogdanov, Photon. Nanostruct.: Fundam. Appl. **52**, 101084 (2022).
12. P. M. Piechulla, B. Fuhrmann, E. Slivina, C. Rockstuhl, R. B. Wehrspohn, and A. N. Sprafke, Adv. Opt. Mater. **9**, 2170068 (2021).
13. W. Man, M. Florescu, K. Matsuyama, P. Yadak, G. Nahal, S. Hashemizad, E. Williamson, P. Steinhardt, S. Torquato, and P. Chaikin, Opt. Express **21**, 19972 (2013).
14. A. D. Sinelnik, I. I. Shishkin, X. Yu, K. B. Samusev, P. A. Belov, M. F. Limonov, P. Ginzburg, and M. V. Rybin, Adv. Opt. Mater. **8**, 2001170 (2020).
15. P. Wang, Y. Zheng, X. Chen, C. Huang, Y. V. Kartashov, L. Torner, V. V. Konotop, and F. Ye, Nature (London, U.K.) **577**, 42 (2020).
16. N. Lassaline, R. Brechbühler, S. J. Vonk, K. Ridderbeek, M. Spieser, S. Bisig, B. le Feber, F. T. Rabouw, and D. J. Norris, Nature (London, U.K.) **582**, 506 (2020).
17. L. Maiwald, T. Sommer, M. S. Sidorenko, R. R. Yafyasov, M. E. Mustafa, M. Schulz, M. V. Rybin, M. Eich, and A. Y. Petrov, Adv. Opt. Mater. **10**, 2100785 (2022).
18. V. A. Chistyakov, M. S. Sidorenko, A. D. Sayanskiy, and M. V. Rybin, Phys. Rev. B **107**, 014205 (2023).
19. K. C. Neuman and S. M. Block, Rev. Sci. Instrum. **75**, 2787 (2004).
20. K. X. Wang, Z. Yu, V. Liu, A. Raman, Y. Cui, and S. Fan, Energy Environ. Sci. **7**, 2725 (2014).
21. T. M. Mercier, T. Rahman, C. Krishnan, E. Khorani, P. J. Shaw, M. E. Pollard, S. A. Boden, P. G. Lagoudakis, and M. D. Charlton, Nano Energy **84**, 105874 (2021).
22. C. Guo, T. Sun, F. Cao, Q. Liu, and Z. Ren, Light Sci. Appl. **3**, e161 (2014).
23. R. Saive, Prog. Photovolt.: Res. Appl. **29**, 1125 (2021).
24. P. W. Anderson, Phys. Rev. **109**, 1492 (1958).
25. S. John, Phys. Rev. Lett. **58**, 2486 (1987).
26. L. Levi, M. Rechtsman, B. Freedman, T. Schwartz, O. Manela, and M. Segev, Science (Washington, DC, U. S.) **332**, 1541 (2011).
27. A. Petrov, private commun. (2021).
28. L. Maiwald, S. Lang, D. Jalas, H. Renner, A. Y. Petrov, and M. Eich, Opt. Express **26**, 11352 (2018).
29. Y. Kim, M. M. Tentzeris, and S. Lim, Materials **12**, 402 (2019).
30. G. Boussatour, P.-Y. Cresson, B. Genestie, N. Joly, and T. Lasri, IEEE Microwave Wireless Compon. Lett. **28**, 374 (2018).

Translated by R. Tyapaev